AN INVESTIGATION OF ABLATION BEHAVIOR OF AVCOAT 5026/39M OVER A WIDE RANGE OF THERMAL ENVIRONMENTS

by Roger K. Crouch and Gerald D. Walberg

Langley Research Center
Langley Station, Hampton, Va.

AN INVESTIGATION OF ABLATION BEHAVIOR OF AVCOAT 5026-39/M

OVER A WIDE RANGE OF THERMAL ENVIRONMENTS

By Roger K. Crouch and Gerald D. Walberg

Langley Research Center
Langley Station, Hampton, Va.

NATIONAL AERONAUTICS AND SPACE ADMINISTRATION

AN INVESTIGATION OF ABLATION BEHAVIOR OF AVCOAT 5026-39/M
OVER A WIDE RANGE OF THERMAL ENVIRONMENTS

By Roger K. Crouch and Gerald D. Walberg
Langley Research Center

SUMMARY

Ablation studies have been carried out on the ablation material Avcoat 5026-39/M over a wide range of pressures, heat-transfer coefficients, and oxygen fluxes. The ablation behavior of the material was found to be strongly dependent on the level of heat-transfer coefficient. At values of heat-transfer coefficient less than 0.17 lbm/ft^2-sec (0.83 kg/m^2-sec), measured char recession rates were comparable to those predicted for diffusion-controlled char oxidation. At high values of heat-transfer coefficient, the ablation rate increased rapidly with increasing heat-transfer coefficient and severe mechanical char failure was observed. The structure, composition, and removal rate of the char were significantly influenced by stream oxygen content at low heat-transfer coefficients but not at high heat-transfer coefficients.

Empirical correlations have been found between the mass-loss rate and the heat-transfer coefficient and between the mass-loss rate and a parameter related to the product of oxygen flow to the surface and a reference shear.

INTRODUCTION

The ablation material which comprises the reentry heat shield of the Apollo command module is a low-density glass-filled epoxy-novolac system designated Avcoat 5026-39/HC-G. Numerous investigations of this material have shown that at environmental conditions within the Apollo flight envelope, the material provides efficient thermal protection. Recently, however, ground- and flight-test results have indicated that the material ablates at unexpectedly high rates when exposed to severe reentry environments which produce high pressures (higher than those expected during an Apollo reentry) on the char surface. (See ref. 1.)

In an attempt to achieve an improved understanding of the ablation behavior of this material, a series of studies were carried out in three high-enthalpy wind tunnels at the Langley Research Center on a molded ablator which had the same composition as the Apollo material but which was not fabricated with a honeycomb matrix. These studies

covered ranges of stagnation enthalpy from 900 to 4000 Btu/lbm (2.09 to 9.28 MJ/kg), pressure on the model nose from 0.06 to 14.0 atm, and heating rates from 150 to 1500 Btu/ft^2-sec (1.7 to 17.0 MW/m^2).

<div align="center">SYMBOLS</div>

The units used for the physical quantities defined in this paper are given both in the U.S. Customary Units and in the International System of Units (SI). Factors relating the two systems are given in reference 2.

A,N   constants (see eq. (3))

H_o heat-transfer coefficient, $\dfrac{\dot{q}_{c,s}}{h_s}$, lbm/ft^2-sec   (kg/m^2-sec)

h_s stagnation enthalpy, Btu/lbm   (J/kg)

K   free-stream oxygen mass fraction

l liquid phase

M   Mach number

$\dot{m}_o$ diffusion-controlled mass flux of oxygen to char surface, lbm/ft^2-sec (kg/m^2-sec)

$\dot{m}_{vp}$ steady-state mass-loss rate of virgin plastic, lbm/ft^2-sec   (kg/m^2-sec)

$p_{t,2}$ stagnation pressure behind a normal shock wave, atm (1 atm equals 1.013 × 10^5 N/m^2)

$\dot{q}_c$ local cold-wall (540° R) aerodynamic heating rate, no blowing, Btu/ft^2-sec (W/m^2)

$\dot{q}_{c,s}$ stagnation-point cold-wall (540° R) aerodynamic heating rate, no blowing, Btu/ft^2-sec   (W/m^2)

r_n effective nose radius of model, ft   (m)

s   solid phase

2

T_W char surface temperature, degrees Rankine (degrees Kelvin)

t time of model exposure to test stream, sec

u_e local flow velocity parallel to char surface at outer edge of boundary layer, ft/sec (m/sec)

u_∞ free-stream velocity ahead of shock, ft/sec (m/sec)

ρ_{vp} density of undegraded material (virgin plastic), lbm/ft^3 (kg/m^3)

τ aerodynamic shear stress, lbf/ft^2 (N/m^2)

τ_r reference shear (see eq. (8)), lbf/ft^2 (N/m^2)

FACILITIES, MODELS, AND TEST PROCEDURES

Facilities and Test Conditions

The investigation was carried out over a wide range of conditions which were obtained by using three environmental test facilities. A brief description of the facilities and the test environments obtained in each is outlined in the following paragraphs. The specific environmental conditions of each test run are listed in table I.

Langley 20-inch hypersonic arc-heated tunnel.- The Langley 20-inch hypersonic arc-heated tunnel consists of a magnetically rotated dc electric arc which heats a test stream of either air or nitrogen. The heated gas is then expanded through a conical nozzle to a nominal Mach number of 5.0. (See ref. 3.) When an air stream was utilized, the arc chamber pressure was set at a value of either 90 psia (6.1×10^5 N/m²) or 200 psia (1.3×10^6 N/m²), and these pressures result in stagnation pressures on the model nose of approximately 0.06 atm or 0.14 atm, respectively. The enthalpy of the stream was approximately 4000 Btu/lbm (9.28 MJ/kg) for the lower pressure and approximately 3000 Btu/lbm (6.96 MJ/kg) for the higher pressure. The resultant heating rate, as measured by a 1-inch-diameter (2.5-cm) flat-faced calorimeter, was about 120 Btu/ft²-sec (1.36 MW/m²) for both pressures. However, when a nitrogen stream was utilized, the arc was stable only at the chamber-pressure setting of 200 psia (1.3×10^6 N/m²). At this chamber pressure, the stagnation pressure on the model was about 0.15 atm and the enthalpy was about 3800 Btu/lbm (8.8 MJ/kg). These values resulted in a heating rate, as measured by the calorimeter, of approximately 160 Btu/ft²-sec (1.8 MW/m²).

Langley 11-inch ceramic-heated tunnel.- The Langley 11-inch ceramic-heated tunnel described in reference 4 consists of a large bed (approximately 20 feet or 6.1 meters thick) of ceramic pebbles which were preheated to a temperature of either 3000° R (1670° K) or 4000° R (2220° K). An air stream passes through the bed and exits through a nozzle affixed to the vessel containing the ceramic pebbles. At a Mach number of 6, the test stream has an enthalpy of approximately 1100 Btu/lbm (2.55 MJ/kg) for a 4000° R (2220° K) bed temperature and a stagnation pressure on the model of 1.1 atm for a bed pressure of 900 psia (6.2×10^6 N/m^2) and 1.7 atm for a bed pressure of 1100 psia (7.6×10^6 N/m^2). The cold-wall heating rate for the lower pressure case, as measured by a 1-inch-diameter (2.5-cm) thin-wall hemispherical calorimeter, is approximately 170 Btu/ft^2-sec (1.93 MW/m^2).

Modification of the facility for use with a Mach number 2 nozzle gives a stream with an enthalpy of approximately 1150 Btu/lbm (2.67 MJ/kg) for a 4000° R (2220° K) bed temperature and about 850 Btu/lbm (1.97 MJ/kg) for a 3000° R (1670° K) bed temperature. The stagnation pressure on the model can be varied from about 5 atm to 14 atm by changing the stagnation pressures of the bed. Heating rates calculated by the method of Fay and Riddell (ref. 5) are within 10 percent of calorimeter measurements from previous tests and are about 500 Btu/ft^2-sec (5.7 MW/m^2) for 1-inch-diameter (2.5-cm) hemispheres in the higher enthalpy and the lowest pressure environment.

Arc-heated materials jet.- The arc-heated materials jet at the Langley Research Center (ref. 6) like the hypersonic tunnel has a magnetically rotated dc electric arc which heats the test stream before expansion through a conical nozzle with an exit diameter of 0.75 inch (1.9 cm). This facility provides a stream at a Mach number of 2 with an enthalpy which can be varied from 1000 to 2000 Btu/lbm (2.3 to 4.6 MJ/kg) by varying the power input to the arc. The stagnation pressure on the model is held virtually constant at about 5 atm. The heating rates calculated by the method of Fay and Riddell (ref. 5) again are within 10 percent of calorimeter measurements from previous tests at various enthalpies. The gas composition of the stream in this facility can be varied by any increment from a pure nitrogen stream to a pure air stream by premixing of the gas supply.

Models

The ablation material used for the reentry heat shield of the Apollo command module is an epoxy-novolac resin system which is 25-percent (by weight) fibrous filler and 30-percent (by weight) phenolic Microballoons. The fibrous filler consists of equal parts of chopped silica fibers (nominal length of 1/4 inch or 0.6 cm) and milled E-glass. This material is gunned into a honeycomb matrix (cell diameter of 3/8 inch or 0.95 cm) which is a fiber glass impregnated with a basic nylon-phenolic resin and dip coated with

polyester. The material has an average density of about 33 lbm/ft^3 (5.3×10^2 kg/m^3) and is designated Avcoat 5026-39/HC-G.

The models used in this investigation had a maximum diameter of 1 inch (2.5 cm) which precluded the use of the honeycomb-matrix material. All models were made from two blocks of molded material (Avcoat 5026-39/M). The molded material has the same composition as Avcoat 5026-39/HC-G, but it does not contain the honeycomb matrix. This difference in material could be significant; however, data trends should be the same for both materials. Models for the tests in the hypersonic tunnel and the ceramic-heated tunnel were made from the same block of material with a measured density of 39 lbm/ft^3 (6.2×10^2 kg/m^3). Models for the tests in the arc jet were made from a different block of material with a density of 30 lbm/ft^3 (4.8×10^2 kg/m^3). Density variations in models from the same block were small.

Photographs of typical models before being tested in the hypersonic tunnel, the ceramic-heated tunnel at a Mach number of 6, and the arc jet are shown in figure 1(a). These hemisphere-cylinder models of Avcoat 5026-39/M were bonded to a mild-steel sting by a high-temperature bonding resin. Models were made with nose radii of 1/2, 3/8, 1/4, 3/16, and 1/8 inch (1.3, 0.9, 0.6, 0.4, and 0.3 cm). Models used for a limited number of tests in the ceramic-heated tunnel at a Mach number of 2 were 1/2-inch-diameter (1.3-cm) cylinders with 45° half-angle cones. These models were threaded on the back for bonding to a mild-steel sting. (See fig. 1(b).)

Procedures

Such parameters as pressure, enthalpy and heating rate, and oxygen content of the stream were varied in an attempt to separate the effects of these parameters on the behavior of the material. Models of different nose radii were run in the three facilities (ceramic-heated tunnel at a Mach number of 6) at a given pressure and enthalpy. Also models were run in the ceramic-heated tunnel at a Mach number of 2 over a wide range of pressures. Information on the influence of oxygen content of the stream on the models was obtained in the arc jet and the hypersonic tunnel.

The general procedure for tunnel operation was first to activate the tunnel and allow it to reach a steady-state flow situation. Any loose dust in the ceramic-heated tunnel was thus removed. The model was inserted into the stream for a predetermined length of time and withdrawn. The tunnel was then shut down in a normal fashion. The test runs in the hypersonic tunnel were slightly different in that a calorimeter was inserted into the stream and then retracted 2 seconds before and after the model was in the stream. This action bracketed the heating rate on the model during the run. No calorimeters were used in the arc jet and the ceramic-heated tunnel during a model test run. Repeatability of the

test conditions were approximately ±5 percent for the ceramic-heated tunnel and the hypersonic tunnel and approximately ±10 percent for the arc jet.

Each model was photographed during the test runs by high-speed Milliken cameras operating at 400 frames per second. A photographic pyrometer similar to that described in reference 7 recorded the surface temperature of each model during the test runs.

DISCUSSION AND ANALYSIS OF RESULTS

Presentation of Results

The data obtained for each test run are presented in table I. Runs 1 to 8 were in the hypersonic tunnel, runs 9 to 12 were in the ceramic-heated tunnel at a Mach number of 6, runs 13 to 16 were in the ceramic-heated tunnel at a Mach number of 2, and runs 17 to 30 were in the arc jet. The values for stagnation enthalpy h_s are considered to be accurate to within 10 percent. For the hypersonic tunnel, the stagnation-point cold-wall heating rates $\dot{q}_{c,s}$ are the measured values, but for the ceramic-heated tunnel and the arc jet, they are calculated values corrected to correspond to the nose radius of the model being tested. The heat-transfer coefficients H_O were calculated for the corresponding nose radii by the method of Fay and Riddell (ref. 5):

$$H_O \equiv \frac{\dot{q}_{c,s}}{h_s} \tag{1}$$

In table I, the values of nose radii r_n for runs 1 to 12 and runs 17 to 30 are the nose radii of the hemisphere-cylinder models before the test runs. Study of the high-speed motion pictures taken of runs 13 to 16 indicated that these models, which were initially cone-cylinders, assumed a relatively constant blunt-body shape soon after entering the stream (less than 0.125 second). The nose radii were measured from the motion pictures, were corrected for bluntness (see ref. 8), and are listed in table I.

As previously mentioned, a photographic pyrometer was used to monitor the surface temperature T_w of each model. The surface temperatures of most of these models had an irregular distribution because of spallation, which is discussed in greater detail in a later section. Variations of up to 600° R (330° K) in small adjacent areas were often seen. Therefore, it was very difficult to define wall temperatures for the models. Each value listed in table I is an average of several values read from the surface of the model. In some cases, the wall temperatures exceeded the range of the photographic pyrometer, and these values are indicated as having been greater than the maximum value that could have been read from that film.

The values for mass-loss rate of virgin plastic $\dot{m}_{vp}$ were obtained by measuring the recession rate of the stagnation region of the models from the high-speed motion

pictures. This linear recession per unit time was then multiplied by the appropriate density factor to obtain the mass-loss rate of the virgin material. This procedure is based upon the assumption of steady-state ablation which implies a constant char thickness throughout the run. The assumption of steady-state ablation is acceptable for most of the present test runs, because the models exhibited large recession rates and thin char layers. However, the models run in the hypersonic tunnel did not recede rapidly, and hence, the assumption is questionable. Therefore, in table I the values of $\dot{m}_{vp}$ for the hypersonic tunnel should be treated as relative indications of recession rate rather than as accurate measures of virgin-plastic ablation rate.

Analysis of Visual Observations

Study of the model appearance during and after the tunnel tests led to a cursory conclusion that three parameters seem to effect the biggest changes in material behavior. They are (1) the heat-transfer coefficient, (2) the stagnation pressure on the model, and (3) the oxygen mass fraction of the stream (and correspondingly the oxygen flux to the surface of the model).

Effect of heat-transfer coefficient and stagnation pressure on material behavior.- The heat-transfer coefficients during this investigation were varied from about 0.04 to 0.96 lbm/ft^2-sec (0.20 to 4.7 kg/m^2-sec) by varying the model nose radius and test conditions. Over this range, many variations in material behavior were apparent. In figure 2, photographs are presented of three models which were tested at the same low pressure and oxygen mass fraction but at different heat-transfer coefficients. Since these models had the same initial length, the difference in the amount of material lost during the runs is immediately apparent from the photographs. Study of the high-speed motion pictures taken of these models during the test runs indicates that the model of largest diameter (fig. 2(c)) lost no pieces of solid char, but both the other models (figs. 2(a) and (b)) lost small pieces (spallation) sporadically, the smaller model doing so more frequently (a piece about every 0.0025 second). The temperature in the stagnation region of these models was very uniform. Also, a significant amount of glass accumulation on each model was apparent. When the models were cross sectioned, the char thickness of each was found to be on the order of 0.1 inch (0.3 cm).

Photographs of three models tested at a higher pressure of about 1 atm are presented in figure 3. Again the recession rates increased with increasing heat-transfer coefficient. No change in the spallation frequency was observed, and the frequency appeared to be essentially the same as that for the smallest model shown in figure 2. The amount of glass accumulation on the models appeared to decrease as the heat-transfer coefficient increased. The char thickness of each model also tended to decrease with

increasing H_O, the thickness being on the order of 0.02 inch (0.05 cm) for the largest model (fig. 3(a)) and practically zero for the smallest model (fig. 3(c)).

High-speed motion pictures of the two smaller models in this environment and all models tested in the more severe environments ($H_O > 0.3$ lbm/ft^2-sec or 1.5 kg/m^2-sec) showed regions on the model surface which were much cooler than the rest of the surface. These cooler areas appeared where spallation had just occurred and disappeared rapidly. For the models in the more severe environments, these cool areas sometimes covered more than half of the total surface of the models. Study of the surface temperatures of these models, as recorded on the film of the photographic pyrometer, seems to indicate that these apparently cooler areas were lower in temperature than the rest of the surface by about 400° to 800° R (220° to 440° K) but were still around 3000° R (1670° K). It is believed that these areas were the cooler regions of the char exposed by the spallation. The spallation seemed to be random with respect to both location on the model surface and time.

Figure 4 shows two models tested at a pressure of about 14 atm. It should be noted that even though these models had about the same heat-transfer coefficient, the model with the higher $\dot{q}_{c,s}$ receded at a higher rate. This difference in recession rate indicates a dependency of recession on $\dot{q}_{c,s}$. These models exhibited the cool areas on the surface, the lower amounts of glass accumulation, and the extremely thin char layers characteristic of these more severe environments. The spallation frequency of the models in these environments was very high, several pieces coming off during each motion-picture frame (2.5×10^{-3} second). This rapid spallation is illustrated by the photograph presented in figure 5.

It should be noted that at a given pressure, the heat-transfer coefficient was varied by changing the model nose radius. However, in the facilities used for these tests, it was impossible to change the pressure without changing the heat-transfer coefficient. Therefore, in this section no comparisons are made for models tested at different stagnation pressures, even though the heat-transfer coefficients were different.

In summary, a strong relationship appears to exist between the mass-loss rate and the heat-transfer coefficient. However, at a given heat-transfer coefficient, the heating rate also appears to have a marked influence upon the mass-loss rate. This result implies the possibility that mass-loss rate is dependent upon the product of these two parameters. This possibility is discussed subsequently.

Effect of oxygen mass fraction of the stream on material behavior.- Models tested in a stream held at a constant low-pressure level are shown in figure 6. The model in figure 6(a) was tested in a pure nitrogen stream, and the model in figure 6(b) was tested in an air stream. The difference in length is immediately apparent as well as a difference

in appearance. The model in figure 6(a) did not spall during the run and lost a negligible amount of material; however, the model in figure 6(b) spalled sporadically during the run and lost about 0.4 inch (1 cm) of material. Also, there was a large amount of glass accumulation on the model tested in air, but practically no glass accumulation on the model tested in nitrogen; however, microscopic study of the chars revealed the presence of small beads of glass on or near the surface of the model tested in nitrogen.

Figure 7 shows the comparative char thickness for two models tested at this low-pressure condition in an air stream and a nitrogen stream. As an aid in interpreting figure 7, dashed white lines have been drawn along the interface between the virgin plastic and the pyrolysis zone. It is pointed out that the model run in air, aside from having a much thinner char than the one run in nitrogen, also appears to have a slightly different char structure. The model run in air has a pyrolysis zone where the char consists of mostly glass fibers and a very soft carbon structure. Above this region, the char is lighter in color and seems to be relatively firm. The outer region is black and firm. The models run in nitrogen have essentially the same char built-up pattern (that is, the soft carbonaceous region with its glass fibers; the lighter, firmer region where the glass fibers are not so prevalent; and the black, firm region), but in addition, they have an outer region which is a lighter gray, not as dense or thick as the previous region, and not as strong. Also, referring back to figure 6(a), a dark circular zone is seen on the nose of the model.

Several investigators have studied the chemistry of chars containing silicon dioxide (SiO_2) and have shown that at the temperatures existing near the char surface, a reaction producing silicon carbide (SiC) is possible. (See refs. 9 and 10.) On the basis of the conclusions of these investigators and the appearance of the models tested in the present investigation, the following char structure for models run in nitrogen is postulated:
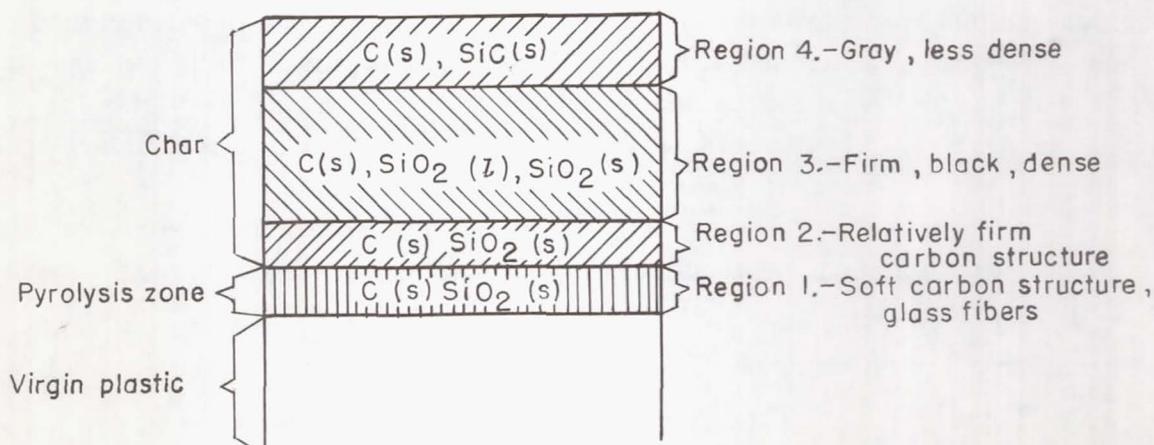
The virgin material pyrolyzes to form a carbon char which contains SiO_2 fibers (regions 1, 2, and 3). The silica fibers subsequently melt and react with the carbon to produce SiC. On the basis of the data presented in reference 10 and the amount of SiO_2 present in the 5026-39/M material, the preferred reaction could be

$$SiO_2 + 3C \rightarrow SiC + 2CO \tag{2}$$

The CO is given off with the pyrolysis gases, and, as a result, the char is less dense. The gray SiC is distributed throughout the basically carbon char to give a grayish tint such as was observed in the test models.

Although this postulated mechanism seems to account for the char structure in the nitrogen runs, it does not describe the chars produced in air. The models tested in air produced chars that contained regions 1, 2, and 3 but did not contain region 4. The data presented in reference 10 show that at typical char surface temperatures, the rates of the SiC reactions are relatively slow. The models tested in air have thinner char layers and faster recession rates than the models tested in nitrogen. Hence, the possibility exists that during the test runs in air, the SiO_2 and C do not react significantly because of the shorter time that they are in contact at high temperatures. The relatively slow rates of these reactions could also account for the fact that there is practically no difference in the char structures produced in the more severe flow environments where the recession rates are high regardless of the stream oxygen content.

Figure 8 shows the effects of oxygen mass fraction at a high-pressure level of about 5 atm. All the models were very similar in behavior during the runs; they spalled continuously throughout the run and receded about the same amount in spite of the large differences in oxygen flux. The appearances of the models seem to be the same with the exception of the presence of a glass accumulation on the model tested in air (fig. 8(c)). The model tested in nitrogen (fig. 8(a)) has what appear to be glass fibers visible on the surface, and a microscopic examination of the surface showed small globules of glass to be present. The model tested in a stream consisting of equal parts of nitrogen and air (fig. 8(b)) also, has visible glass fibers with a few relatively large drops of glass scattered over the surface. The glass fibers do not seem as prominent on the surface of the model tested in air. The char thickness on these runs is very thin (<0.01 inch or 0.03 cm) and could not be measured. Therefore, other than the difference in the glass accumulation, no indications of a chemical reaction between the glass fibers and the char are present in these environments.

In summary, the following observations are made with respect to the effect of the stream oxygen mass fraction upon the material behavior:

(1) At high heat-transfer coefficients ($H_O > 0.3$ lbm/ft^2-sec or 1.5 kg/m^2-sec) and correspondingly high pressures, the stream composition has very little effect on the recession rate. (Compare with section "Empirical Correlations of the Data.")

(2) At low heat-transfer coefficients ($H_O < 0.3$ lbm/ft^2-sec or 1.5 kg/m^2-sec) and correspondingly low pressures, the oxygen mass fraction has a great effect on the recession rate, an increase in oxygen resulting in an increase in the recession rate.

(3) At low heat-transfer coefficients, the char structure of models tested in a nitrogen stream differs significantly from that of models tested in an air stream and suggests the possibility of chemical reactions between the C(s) char and SiO$_2(l)$ to produce SiC(s).

(4) At low heat-transfer coefficients, models tested in a nitrogen stream never have a glass accumulation on the surface, whereas models tested in an air stream always have a relatively large amount of glass on the surface.

Spallation.- As stated previously, almost all the models tested in this series spalled. This spallation generally occurred in the form of small pieces leaving the model surface in a random fashion with varying frequencies depending upon the severity of the environment. The surface temperature was cooler in the vicinity of the spallation by about 600° R (330° K).

This type of spallation appears to be different from that described by Scala and Gilbert (ref. 11). According to Scala and Gilbert, the entire char layer is periodically removed when failure occurs at the pyrolysis interface as a result of internal-pressure buildup and thermal stress. However, one apparent instance of this type of failure was observed. The model being tested was a 0.75-inch-diameter (1.9-cm) hemisphere-cylinder of the lower density material. The test was carried out in the arc jet which has a nozzle with an exit diameter of only 0.75 inch (1.9 cm), and the model was initially 0.25 inch (0.6 cm) from the nozzle. The repeatability of the tests in this facility was rather poor, and the possibility exists that some size effect caused by the relatively large model may have given anomolous results. The apparent internal-pressure failure occurred during run 23. The environment was one of the least severe attainable in the arc jet with respect to the heat-transfer coefficient. The model appeared to behave in much the same fashion as other models tested in this facility except that the frequency for the loss of small pieces was much lower. After the model had been in the stream for about 1 second, the entire char layer was removed from the surface in less than 0.0025 second. The model surface temperature dropped from about 3700° R (2050° K) to less than 2500° R (1390° K), and the model length was shortened by about 0.1 inch (0.25 cm). The model reheated quickly and exhibited the same behavior again about 1 second later, except the length change was slightly less. At the end of the run, another

11

large piece of char was removed, but this occurrence took place as the model was being withdrawn from the stream and quite possibly was not spontaneous. Since this behavior was exhibited only by one model and since the test conditions were far from ideal, it must be stated again that whether this behavior is characteristic of the material in this particular environment or was a spurious behavior caused by undesirable test conditions is not known.

Empirical Correlations of the Data

The generally accepted mechanisms of char removal are oxidation of the char, erosion of the char by aerodynamic force, failure due to an internal-pressure buildup, or various combinations of these mechanisms. The present data are not capable of defining the basic mechanisms responsible for the ablation behavior of Avcoat 5026-39/M; however, they can be used to formulate empirical ablation-rate correlations. Several such correlations are discussed in this section.

Since solid pieces of char were lost from almost every model the data were not expected to correlate with the oxygen flux to the surface. However, because the model behavior showed a relatively strong dependency on oxygen mass fraction at the low heat-transfer coefficients, a check for a correlation of mass-loss rate with the oxygen mass flux to the surface of the model was advisable. Figure 9 shows a plot of the mass-loss rate as a function of the diffusion-controlled oxygen mass flux to the surface of the model. The solid line in figure 9 corresponds to the predicted mass-loss rate as calculated by using the theory of reference 12 for a pure air stream. It is seen that at values of heat-transfer coefficient less than 0.17 lbm/ft^2-sec (0.83 kg/m^2-sec) and $\dot{m}_O$ less than 0.04 lbm/ft^2-sec (0.20 kg/m^2-sec), the test results obtained in air agree fairly well with predicted rate; however, for the higher heat-transfer coefficients, the mass-loss rates are much higher than the predicted oxidation rates.

Since the oxidation mechanism is obviously not the only important char-removal mechanism in these tests at the higher heat-transfer coefficients and since an analysis of the data in terms of the other char-removal mechanisms would require assumptions that would make the results doubtful anyway, the decision was made to attempt an empirical correlation of the data.

Previously, it has been hypothesized that some mechanism directly dependent upon the stagnation pressure may be predominant in the removal of the char from the honeycomb version of this material. (See ref. 1.) In reference 13, a pressure effect is proposed in which the external pressure field around a charring ablator causes the pyrolysis gases to flow laterally in the char. It is pointed out in reference 13 that this effect would become more pronounced as the external pressure is increased and as the model size is decreased and, under severe conditions, could result in a flow of boundary-layer gases

12

into the char with an associated increase in heating rate and oxygen flux to the char surface. Therefore, in figure 10, the mass-loss rate for the series of test runs is plotted as a function of stagnation pressure. Some correlation seems to exist between these two parameters. However, at a given pressure, a significant variation is seen in $\dot{m}_{vp}$, and this variation indicates that some of the other char-removal mechanisms are acting on the models. At pressures near 5 atm, models tested in nitrogen and in air receded at comparable rates. Hence, at these high pressures, the char-removal rates seem to depend more on some mechanical failure mechanism than on the oxygen flux to the char surface. This conclusion is also illustrated by the data in figure 9. It should be noted, however, that a pressure effect such as that proposed in reference 13 could have influenced the conditions under which the char recession rates measured in air in the present tests initially deviated from those predictable by one-dimensional steady-state ablation theory ($\dot{m}_o > 0.04$ lbm/ft^2-sec or 0.20 kg/m^2-sec in fig. 9).

Attempts to correlate the data as a function of wall temperature were completely unsuccessful.

Since the mass-loss rates varied greatly at a given pressure (see fig. 2) and since this variation was a function of the heat-transfer coefficient, the decision was made to attempt a correlation directly between the mass-loss rate and the heat-transfer coefficient. Of the equation forms tried (polynomials and power functions), an equation of the form

$$\dot{m}_{vp} = AH_o^N \tag{3}$$

was found to give the apparent best fit to the data. The values of A and N were found by applying a linear best-fit curve through the data on a log-log plot by the method of least squares. Equation (3) with the appropriate values of A and N is shown in figure 11. The data obtained in the stream with the lower concentration of oxygen and in the stream of pure nitrogen seemed generally to fall below the line; thus, an attempt was made to find the relationship between these two parameters $\dot{m}_{vp}$ and H_o for a given mass fraction of oxygen in the stream. The data for all the runs in an air stream (K = 0.232) are presented in figure 12 along with a plot of equation (3) with the appropriate values of A and N. All these runs except run 30 were with the material having a density of 39 lbm/ft^3 (6.2×10^2 kg/m^3). This curve appears to give a qualitative description of this series of test runs. When this type of fit was applied to the data from the other oxygen concentrations, N was found to be a function of oxygen concentration, but these data did not cover a wide enough range or enough points to bring about any conclusions.

However, the study of the air data was carried one step further. The power dependency of $\dot{m}_{vp}$ on H_o was relatively close to a value of 1.5. If Reynold's analogy for a relationship between heat-transfer coefficient and shear stress

$$\tau \propto u_e \frac{\dot{q}_c}{h_s} \tag{4}$$

was valid for these test runs and if the analogy between heat and mass transfer in a laminar boundary layer (ref. 14)

$$\dot{m}_O = KH_O \tag{5}$$

also was valid, a cross product of the diffusion-controlled oxygen flux $\dot{m}_O$ and a reference shear stress τ_r would be proportional to the square root of the cold-wall stagnation-point heating rate multiplied by the heat-transfer coefficient raised to a power of 1.5. That is,

$$\tau \propto u_e \frac{\dot{q}_c}{h_s} = \frac{u_e}{u_\infty} \frac{\dot{q}_c}{\dot{q}_{c,s}} u_\infty \frac{\dot{q}_{c,s}}{h_s} = k\tau_r \tag{6}$$

where

$$k \equiv \frac{u_e}{u_\infty} \frac{\dot{q}_c}{\dot{q}_{c,s}} \tag{7}$$

and

$$\tau_r \equiv u_\infty \frac{\dot{q}_{c,s}}{h_s} \tag{8}$$

Since

$$h_s \approx \frac{1}{2} u_\infty^2 \tag{9}$$

it follows that

$$\tau_r \equiv u_\infty \frac{\dot{q}_{c,s}}{h_s} \propto \sqrt{\dot{q}_{c,s}} H_O^{1/2} \tag{10}$$

Then by using equation (5) a relationship of the following form is obtained:

$$\tau_r \dot{m}_O \propto \sqrt{\dot{q}_{c,s}} H_O^{3/2} \tag{11}$$

With this relationship (eq. (11)) in mind, the decision was made to plot $\dot{m}_{vp}$ as a function of $\sqrt{\dot{q}_{c,s}} H_O^{3/2}$ for all the test runs in an air stream. This plot is shown in figure 13 along with the best-fit line as determined by the method of least squares. This curve seems to give a relatively good qualitative representation of the data and seems to describe the behavior shown by the two models in figure 4 better than the relationship expressed in equation (3); that is, the curve includes the dependency of the heating rate in addition to the dependency of the heat-transfer coefficient.

Since the correlation shown in figure 13 seems to describe the behavior shown in figure 4 and since it offers a possible clue to a physical explanation for the material

14

behavior, it is presented herein, even though it does not seem to give as good a fit overall as the correlation with heat-transfer coefficient. Figure 13 is based on data from the stagnation region where the actual aerodynamic shear stresses are very small; therefore, the mechanism of char removal may involve a weakening of the char by the oxygen to a point at which the small shear stresses can tear off the char. However, the fact that the mass-loss rates for the runs in the arc jet with the lower mass fractions of oxygen do not lie on the correlation parameter curve defined by equation (11) when modified for the changes in oxygen flux indicates that the mass-loss rate is more than just a linear function of the oxygen flux; that is, the values of $\dot{m}_{vp}$ for the tests in a nitrogen stream are not significantly different from those in an air stream. However, for the runs in the hypersonic tunnel, a very distinct dependency exists between the recession and the free-stream oxygen mass fraction. (See fig. 11.)

Thus, from the data available, it seems as if no general equation can be written which will describe the behavior of this material for all types of environments, although two closely related correlations have been found which seem to describe the material behavior qualitatively over a wide range of environments. It must be specifically pointed out that the correlations are only good in a qualitative sense, and the curves are not accurate enough to be used in predicting quantitative results and are only meaningful in that they seem to predict trends.

CONCLUDING REMARKS

Ablation studies of the Avcoat 5026-39/M heat-shield material have been carried out over a wide range of pressures, heat-transfer coefficients, and oxygen fluxes. The data obtained from these studies have been analyzed, and empirical correlations of material mass-loss rates have been obtained. It should be noted that the ground tests were carried out with a material which did not contain the honeycomb matrix found in Avcoat 5026-39/HC-G, the heat-shield material of the Apollo command module. This difference in material could be significant, and caution should be used in applying these correlations to flight data in order to get quantitative values. However, the trends should be the same for both materials. The results of this investigation can be summarized as follows:

1. The ablation behavior of the Avcoat 5026-39/M material was found to be strongly dependent on the level of heat-transfer coefficient H_O. At values of H_O below approximately 0.3 lbm/ft^2-sec (1.5 kg/m^2-sec) (that is, low values of heating rate and pressure), the models exhibited moderate char recession rates which were significantly influenced by the level of oxygen flux to the char surface. For H_O less than 0.17 lbm/ft^2-sec (0.83 kg/m^2-sec), the char-removal rates for the models tested in air were comparable in magnitude to predictions made for diffusion-controlled char oxidation. At high values

of H_O (that is, high values of heating rate and pressure), the ablation rate of the material increased rapidly with increasing heat-transfer coefficient and severe mechanical char failure was observed. Under these severe test conditions, the effect of oxygen flux on char recession was small and, at the highest values of H_O, the measured values of char recession rate greatly exceeded diffusion-controlled oxidation predictions.

2. The structure and composition of the Avcoat 5026-39/M char were found to be significantly influenced by the stream oxygen content in the less severe environments. The char produced in nitrogen exhibited a thin, gray surface layer; the char produced in air did not. The models tested in nitrogen did not exhibit the glassy surface or accumulation found on the models tested in air. A chemical reaction between the glass fibers and the carbon char is postulated which seems to explain the char structure for the test runs in the nitrogen stream. In the more severe environments, the stream oxygen content had very little influence on the char which was very thin but seemed to show the same trend with respect to glass accumulation.

3. Two empirical correlations of the material mass-loss rate have been obtained. The first correlation expresses mass-loss rate $\dot{m}_{vp}$ in terms of the heat-transfer coefficient H_O. The second expresses $\dot{m}_{vp}$ in terms of a correlating parameter which may be interpreted as the product of the diffusion-controlled oxygen flux and a reference aerodynamic shear.

Langley Research Center,
    National Aeronautics and Space Administration,
        Langley Station, Hampton, Va., February 12, 1969,
            124-08-03-05-23.

REFERENCES

1. Brooks, William A., Jr.; Tompkins, Stephen S.; and Swann, Robert T.: Flight and Ground Tests of Apollo Heat-Shield Material. Conference on Langley Research Related to Apollo Mission, NASA SP-101, 1965, pp. 29-44.

2. Mechtly, E. A.: The International System of Units — Physical Constants and Conversion Factors. NASA SP-7012, 1964.

3. Schaefer, William T., Jr.: Characteristics of Major Active Wind Tunnels at the Langley Research Center. NASA TM X-1130, 1965.

4. Trout, Otto F., Jr.: Design, Operation, and Testing Capabilities of the Langley 11-Inch Ceramic-Heated Tunnel. NASA TN D-1598, 1963.

5. Fay, J. A.; and Riddell, F. R.: Theory of Stagnation Point Heat Transfer in Dissociated Air. J. Aeronaut. Sci., vol. 25, no. 2, Feb. 1958, pp. 73-85, 121.

6. Mayo, Robert F.; Wells, William L.; and Wallio, Milton A.: A Magnetically Rotated Electric Arc Air Heater Employing a Strong Magnetic Field and Copper Electrodes. NASA TN D-2032, 1963.

7. Exton, Reginald J.: Theory and Operation of a Variable Exposure Photographic Pyrometer Over the Temperature Range 1800° to 3600° F (1255° to 2255° K). NASA TN D-2660, 1965.

8. Zoby, Ernest V.; Sullivan, Edward M.: Effects of Corner Radius on Stagnation-Point Velocity Gradients on Blunt Axisymmetric Bodies. NASA TM X-1067, 1965.

9. DeSesa, Michael A.; and Perkins, Janet S.: Determination of Temperature Profile in Charred Phenolic Composites by Reconstruction of the Ablation Process. Thermophysics and Temperature Control of Spacecraft and Entry Vehicles, Gerhard B. Heller, ed., Academic Press, 1966, pp. 495-512.

10. Blumenthal, Jack L.; Santy, Myrrl J.; and Burns, Eugene A.: Kinetic Studies of High-Temperature Carbon-Silica Reactions in Charred Silica-Reinforced Phenolic Resins. AIAA J., vol. 4, no. 6, June 1966, pp. 1053-1057.

11. Scala, Sinclaire M.; and Gilbert, Leon M.: Thermal Degradation of a Char-Forming Plastic During Hypersonic Flight. ARS J., vol. 32, no. 6, June 1962, pp. 917-924.

12. Swann, Robert T.: Approximate Analysis of the Performance of Char-Forming Ablators. NASA TR R-195, 1964.

13. Bush, Harold G.; and Dow, Marvin B.: Multidimensional Gas Flow Through Permeable Char Layers and Its Effects on Ablation. NASA TR R-296, 1969.

14. Lees, Lester: Convective Heat Transfer With Mass Addition and Chemical Reactions. Combustion and Propulsion — Third AGARD Colloquium, M. W. Thring, O. Lutz, J. Fabri, and A. H. Lefebvre, eds., Pergamon Press, 1958, pp. 451-498.

TABLE I.- TEST DATA

(a) U.S. Customary Units

Run no.	h_s, Btu/lbm	r_n, in.	$\dot{q}_{c,s}$, Btu/ft²-sec	H_o, lbm/ft²-sec	$p_{t,2}$, atm	K	t, sec	T_w, °R	$\dot{m}_{vp}$, lbm/ft²-sec	Rate of mechanical char failure	Facility (a)
1	4000	0.50	[b]147	0.0369	0.0613	0.232	30	3620	0.00783	No failure	HAHT
2	4000	.25	[b]282	.0705	.0606	.232	30	3830	.0372	Low	HAHT
3	4000	.125	[b]426	.106	.0600	.232	30	4050	.0725	Moderate	HAHT
4	3790	.125	[b]592	.156	.143	.000	30	4180	.0181	Very low	HAHT
5	3160	.375	[b]276	.0873	.136	.232	45	4120	.0285	Low	HAHT
6	3770	.375	[b]347	.0916	.150	.000	45	>4260	.00356	No failure	HAHT
7	3120	.25	[b]353	.115	.139	.232	30	No record[c]	.0388	Low	HAHT
8	3910	.25	[b]423	.108	.155	.000	30	No record[c]	.00767	No failure	HAHT
9	1160	.50	[d]168	.145	1.09	.232	20	3410	.065	Moderate	CHT, M = 6
10	1140	.25	[d]328	.209	1.09	.232	10	3540	.104	Moderate	CHT, M = 6
11	1150	.125	[d]336	.291	1.13	.232	10	3650	.224	Moderate	CHT, M = 6
12	1150	.50	[d]210	.182	1.71	.232	15	3660	.151	Moderate	CHT, M = 6
13	1110	.278	[d]648	.584	5.17	.232	3	3963	.858	High	CHT, M = 2
14	1100	.313	[d]874	.794	10.8	.232	3	4015	1.15	High	CHT, M = 2
15	1110	.284	[d]1060	.960	14.3	.232	2	>3910	2.27	High	CHT, M = 2
16	848	.25	[d]813	.961	14.1	.232	2	3790	1.71	High	CHT, M = 2
17	2110	.25	[d]1330	.632	5.02	.000	3	>4000	.681	High	AHMJ
18	2110	.375	[d]1100	.616	5.02	.000	2	>4000	.339	High	AHMJ
19	1910	.375	[d]996	.522	5.27	.118	2	>4000	.447	High	AHMJ
20	1910	.25	[d]1190	.622	5.27	.118	2	>4000	.915	High	AHMJ
21	1110	.188	[d]800	.718	5.20	.118	2	No record[c]	.576	High	AHMJ
22	1120	.25	[d]692	.624	5.24	.118	3	No record[c]	.777	High	AHMJ
23	1120	.375	[d]567	.508	5.23	.118	3	3680	.492	High	AHMJ
24	1190	.375	[d]612	.512	5.27	.000	3	No record[e]	.621	High	AHMJ
25	1300	.188	[d]938	.722	5.23	.000	2	3585	.525	High	AHMJ
26	1230	.25	[d]774	.628	5.24	.000	2	3690	.561	High	AHMJ
27	1620	.25	[d]1030	.636	5.24	.000	2	>4000	.597	High	AHMJ
28	1400	.25	[d]885	.632	No record[f]	.118	2	>4000	.714	High	AHMJ
29	1910	.188	[d]1400	.736	No record[f]	.118	2	>4000	.837	High	AHMJ
30	1590	.25	[d]1010	.634	No record[f]	.232	2	>4000	.792	High	AHMJ

[a]Facilities included the Langley 20-inch hypersonic arc-heated tunnel (HAHT), the Langley 11-inch ceramic-heated tunnel at a Mach number of 6 or a Mach number of 2 (CHT, M = 6) or (CHT, M = 2), and the arc-heated materials jet at the Langley Research Center (AHMJ).

[b]Measured heating rate.

[c]Estimated temperature greater than 4000° R.

[d]Calculated heating rate.

[e]Estimated temperature greater than 3600° R.

[f]Pressure approximately 5 atm.

TABLE I.- TEST DATA — Concluded

(b) SI Units

Run no.	h_s, MJ/kg	r_n, cm	$\dot{q}_{c,s}$, MW/m²	H_0, kg/m²-sec	$p_{t,2}$, atm	K	t, sec	T_w, °K	$\dot{m}_{vp}$, kg/m²-sec	Rate of mechanical char failure	Facility (a)
1	9.28	1.27	[b]1.67	0.180	0.0613	0.232	30	2010	0.038	No failure	HAHT
2	9.28	.635	[b]3.20	.345	.0606	.232	30	2130	.182	Low	HAHT
3	9.28	.318	[b]4.83	.520	.0600	.232	30	2250	.355	Moderate	HAHT
4	8.81	.318	[b]6.71	.762	.143	.000	30	2320	.089	Very low	HAHT
5	7.33	.953	[b]3.13	.427	.136	.232	45	2290	.139	Low	HAHT
6	8.76	.953	[b]3.93	.448	.150	.000	45	>2370	.017	No failure	HAHT
7	7.25	.635	[b]4.01	.562	.139	.232	30	No record[c]	.190	Low	HAHT
8	9.09	.635	[b]4.80	.529	.155	.000	30	No record[c]	.038	No failure	HAHT
9	2.69	1.27	[d]1.91	.710	1.09	.232	20	1890	.318	Moderate	CHT, M = 6
10	2.64	.635	[d]2.70	1.02	1.09	.232	10	1970	.509	Moderate	CHT, M = 6
11	2.67	.318	[d]3.81	1.42	1.13	.232	10	2030	1.10	Moderate	CHT, M = 6
12	2.67	1.27	[d]2.38	.892	1.71	.232	15	2030	.738	Moderate	CHT, M = 6
13	2.58	.706	[d]8.25	2.86	5.17	.232	3	2200	4.18	High	CHT, M = 2
14	2.56	.795	[d]11.10	3.88	10.8	.232	3	2230	5.64	High	CHT, M = 2
15	2.58	.721	[d]13.50	4.69	14.3	.232	2	>2170	11.9	High	CHT, M = 2
16	1.97	.635	[d]10.00	4.70	14.1	.232	2	2110	8.34	High	CHT, M = 2
17	4.90	.635	[d]15.20	3.09	5.02	.000	3	>2220	3.33	High	AHMJ
18	4.90	.953	[d]12.40	2.52	5.02	.000	2	>2220	1.66	High	AHMJ
19	4.42	.953	[d]11.30	2.55	5.27	.118	2	>2220	2.19	High	AHMJ
20	4.42	.635	[d]13.50	3.04	5.27	.118	2	>2220	4.47	High	AHMJ
21	2.58	.478	[d]9.08	3.51	5.20	.118	2	No record[c]	2.81	High	AHMJ
22	2.59	.635	[d]7.85	3.05	5.24	.118	3	No record[c]	3.80	High	AHMJ
23	2.59	.953	[d]6.44	2.48	5.23	.118	3	2040	2.41	High	AHMJ
24	2.77	.953	[d]6.95	2.50	5.27	.000	3	No record[e]	2.55	High	AHMJ
25	3.01	.478	[d]10.76	3.53	5.23	.000	2	1990	2.57	High	AHMJ
26	2.86	.635	[d]8.87	3.07	5.24	.000	2	2050	2.74	High	AHMJ
27	3.76	.635	[d]11.71	3.11	5.24	.000	2	>2220	2.92	High	AHMJ
28	3.25	.635	[d]10.04	3.09	No record[f]	.118	2	>2220	3.49	High	AHMJ
29	4.42	.478	[d]15.91	3.60	No record[f]	.118	2	>2220	4.09	High	AHMJ
30	3.70	.635	[d]11.54	3.10	No record[f]	.232	2	>2220	3.87	High	AHMJ

[a]Facilities included the Langley 20-inch hypersonic arc-heated tunnel (HAHT), the Langley 11-inch ceramic-heated tunnel at a Mach number of 6 or a Mach number of 2 (CHT, M = 6) or (CHT, M = 2), and the arc-heated materials jet at the Langley Research Center (AHMJ).

[b]Measured heating rate.

[c]Estimated temperature greater than 2220° K.

[d]Calculated heating rate.

[e]Estimated temperature greater than 2000° K.

[f]Pressure approximately 5 atm.
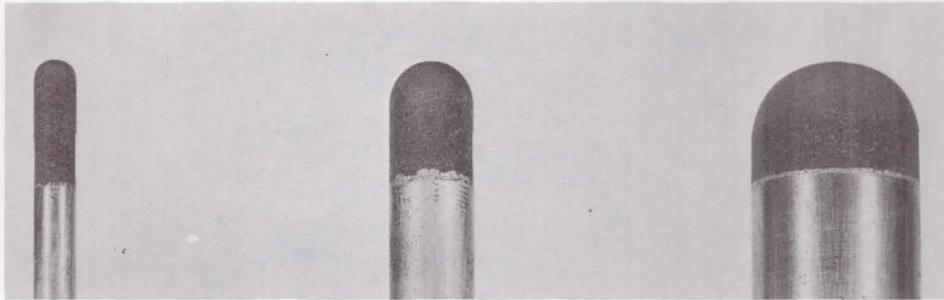
(a) Typical hemisphere-cylinder models.
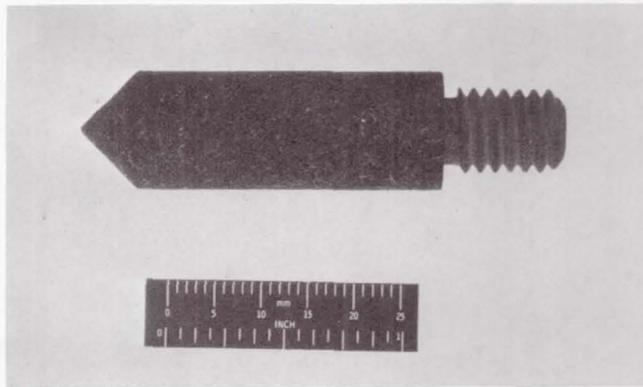
(b) Typical cone-cylinder model for test runs in the ceramic-heated tunnel at a Mach number of 2.

Figure 1.- Model configurations.   L-69-1229

(a) Run 3; H_0 = 0.520 kg/m^2-sec;
run time 30 sec; r_n = 0.3 cm.

(b) Run 2; H_0 = 0.345 kg/m^2-sec;
run time 30 sec; r_n = 0.6 cm.

(c) Run 1; H_0 = 0.180 kg/m^2-sec;
run time 30 sec; r_n = 1.3 cm.

Figure 2.- Models tested at $p_{t,2} \approx 0.06$ atm and K = 0.232.

L-69-1230
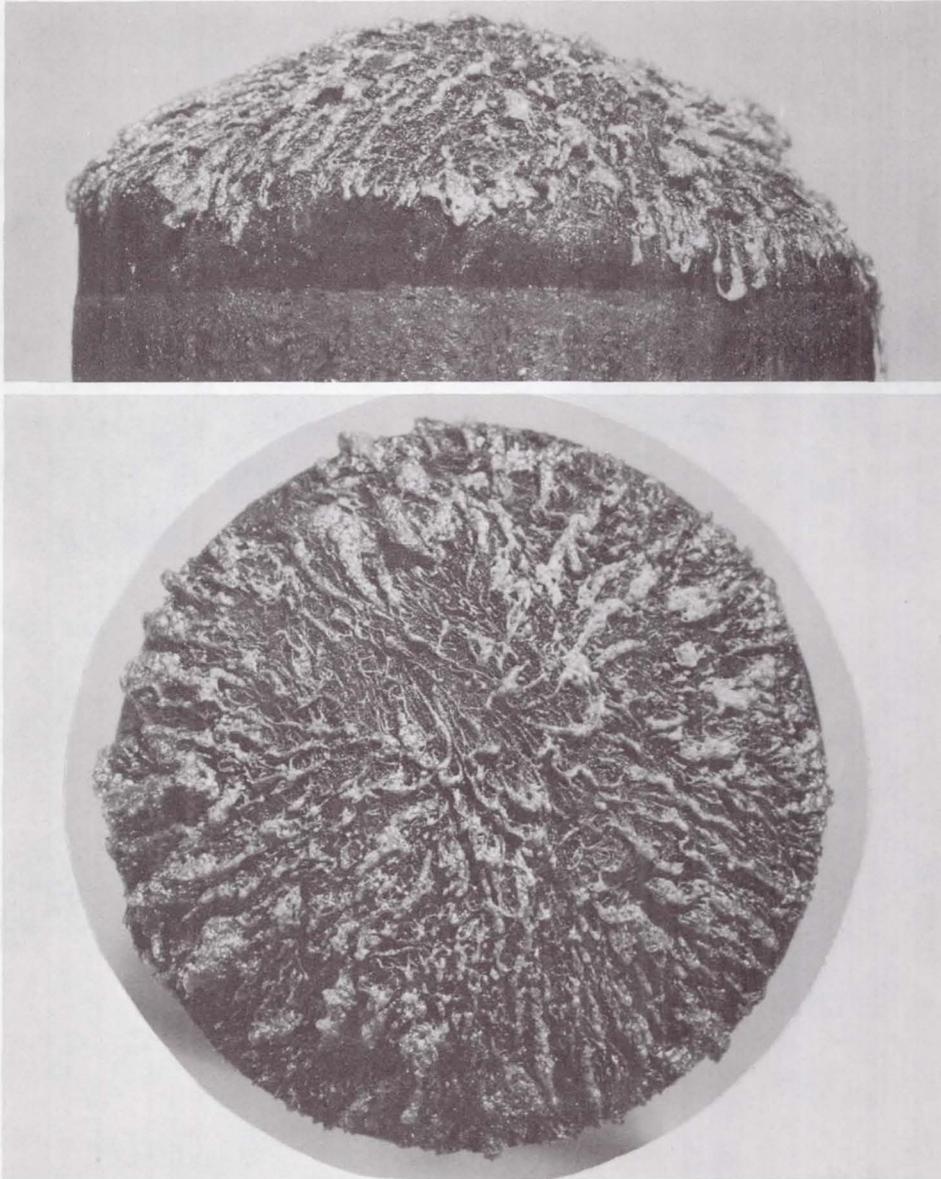
(a) Run 9; $H_0 = 0.710$ kg/m^2-sec; run time 20 sec; $r_n = 1.3$ cm.

Figure 3.- Models tested at $p_{t,2} \approx 1$ atm and $K = 0.232$.   L-69-1231
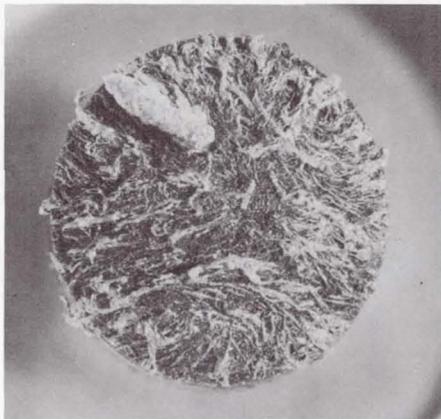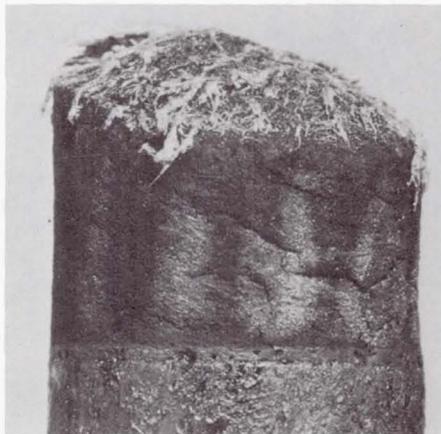
(b) Run 10; H_o = 1.02 kg/m²-sec;
run time 10 sec; r_n = 0.6 cm.
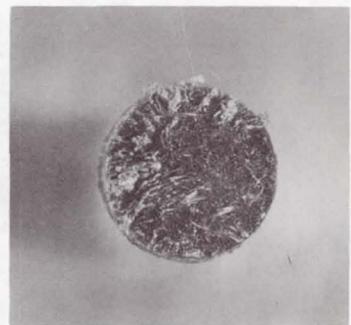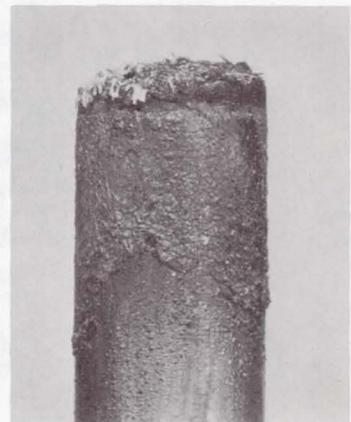
(c) Run 11; H_o = 1.42 kg/m²-sec;
run time 10 sec; r_n = 0.3 cm.

Figure 3.- Concluded.

L-69-1232

(a) Run 15; H_O = 4.69 kg/m^2-sec; run time 2 sec; $\dot{q}_{c,s}$ = 13.5 MW/m^2; h_s = 2.58 MJ/kg.

(b) Run 16; H_O = 4.70 kg/m^2-sec; run time 2 sec; $\dot{q}_{c,s}$ = 10.0 MW/m^2; h_s = 1.97 MJ/kg.

Figure 4.- Models tested at $p_{t,2} \approx$ 14 atm and K = 0.232.

L-69-1233
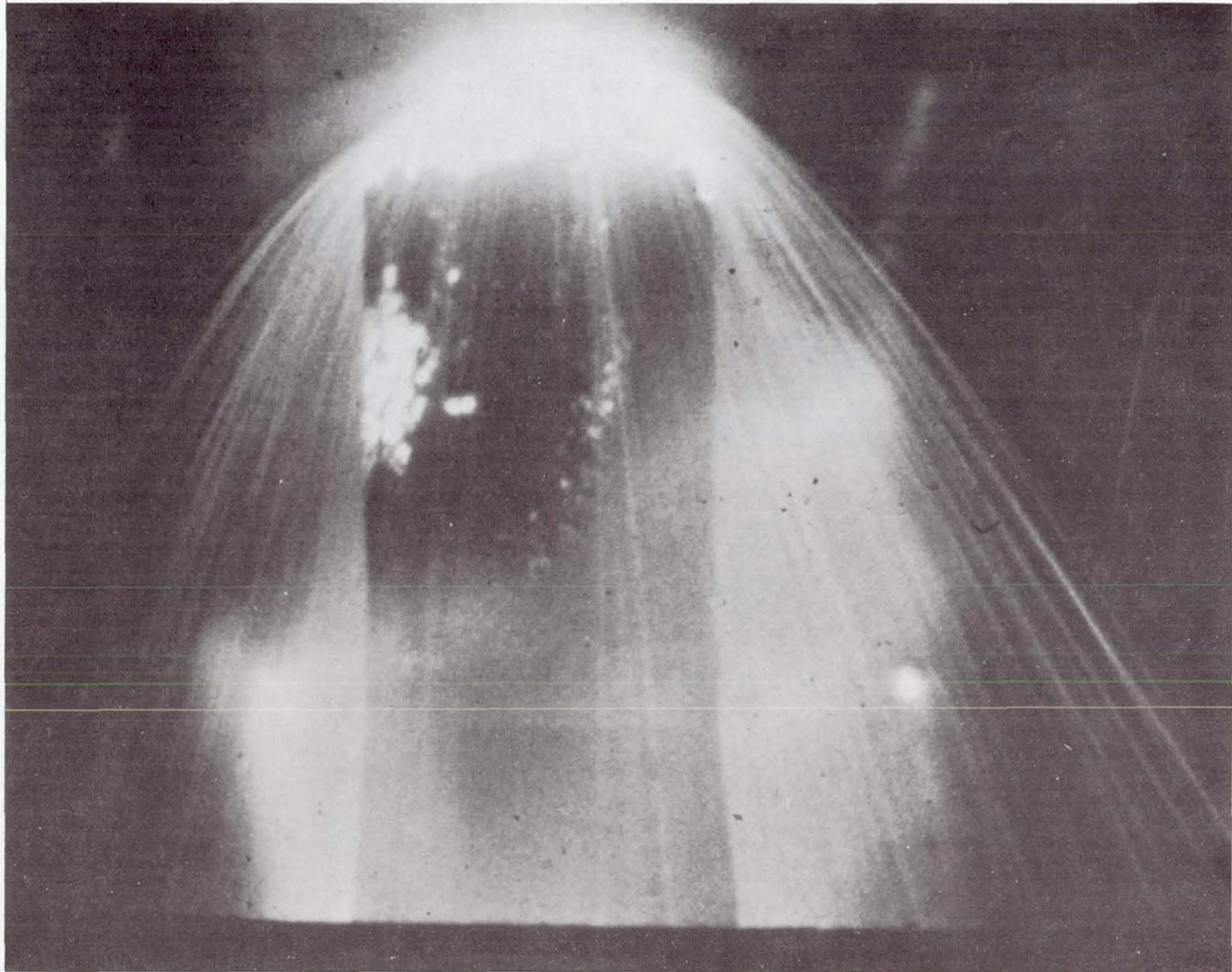
Figure 5.- Typical model spallation during test run in severe environment.

L-69-1234

(a) Run 8; $K = 0.00$; $p_{t,2} \approx 0.15$ atm; $H_0 = 0.529$ kg/m^2-sec; run time 30 sec.

Figure 6.- Effects of oxygen mass fraction on appearance of models at low stagnation pressures and low heat-transfer coefficients.   L-69-1235
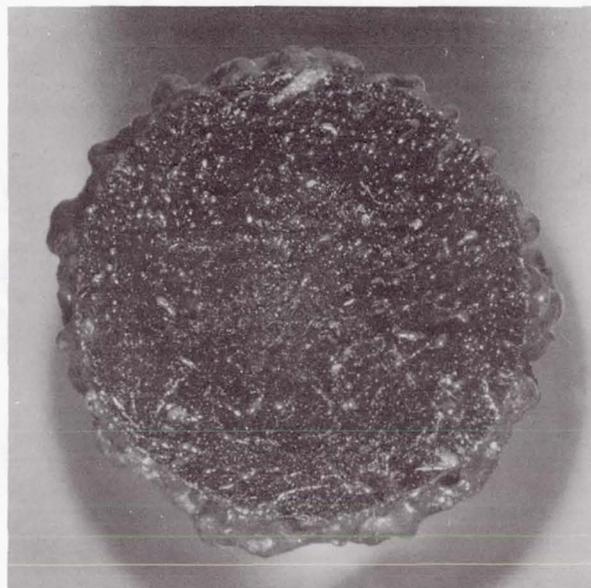
(b) Run 7; $K = 0.232$; $p_{t,2} \approx 0.14$ atm; $H_o = 0.562$ kg/m^2-sec; run time 30 sec.

Figure 6.- Concluded.

L-69-1236
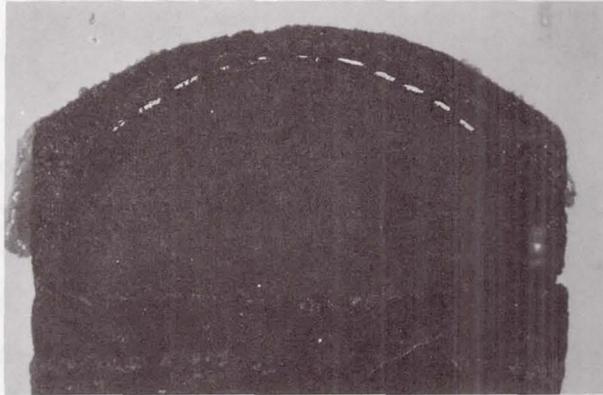
(a) Run 5; K = 0.232; $p_{t,2}$ = 0.136 atm; H_o = 0.427 kg/m^2-sec; run time 45 sec.
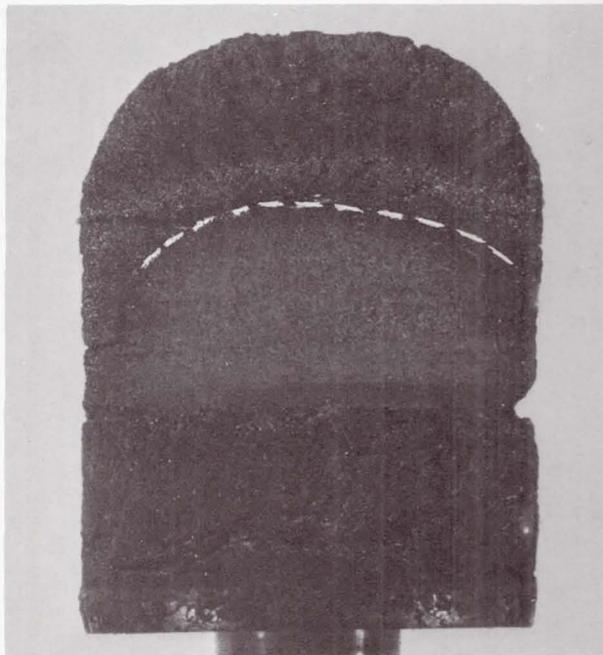
(b) Run 6; K = 0.00; $p_{t,2}$ = 0.15 atm; H_o = 0.448 kg/m^2-sec; run time 45 sec.

L-69-1237

Figure 7.- Effects of oxygen mass fraction on formation of char layers at low stagnation pressures and low heat-transfer coefficients.

(a) Run 27; K = 0.00; $p_{t,2} \approx 5.2$ atm; run time 2 sec; $H_o = 3.11$ kg/m²-sec.
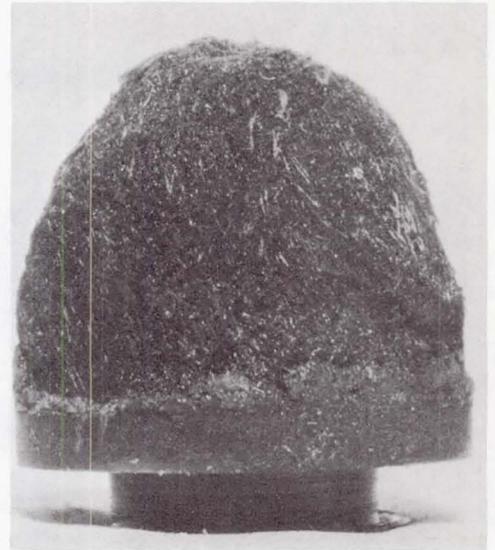
(b) Run 28; K = 0.118; $p_{t,2} \approx 5$ atm; run time 2 sec; $H_o = 3.09$ kg/m²-sec.

(c) Run 30; K = 0.232; $p_{t,2} \approx 5$ atm; run time 2 sec; $H_o = 3.10$ kg/m²-sec.

L-69-1238

Figure 8.- Effects of oxygen mass fraction on appearance of models at high stagnation pressures and high heat-transfer coefficients.

Figure 9.- Mass-loss rate as a function of diffusion-controlled oxygen flux for all test runs.
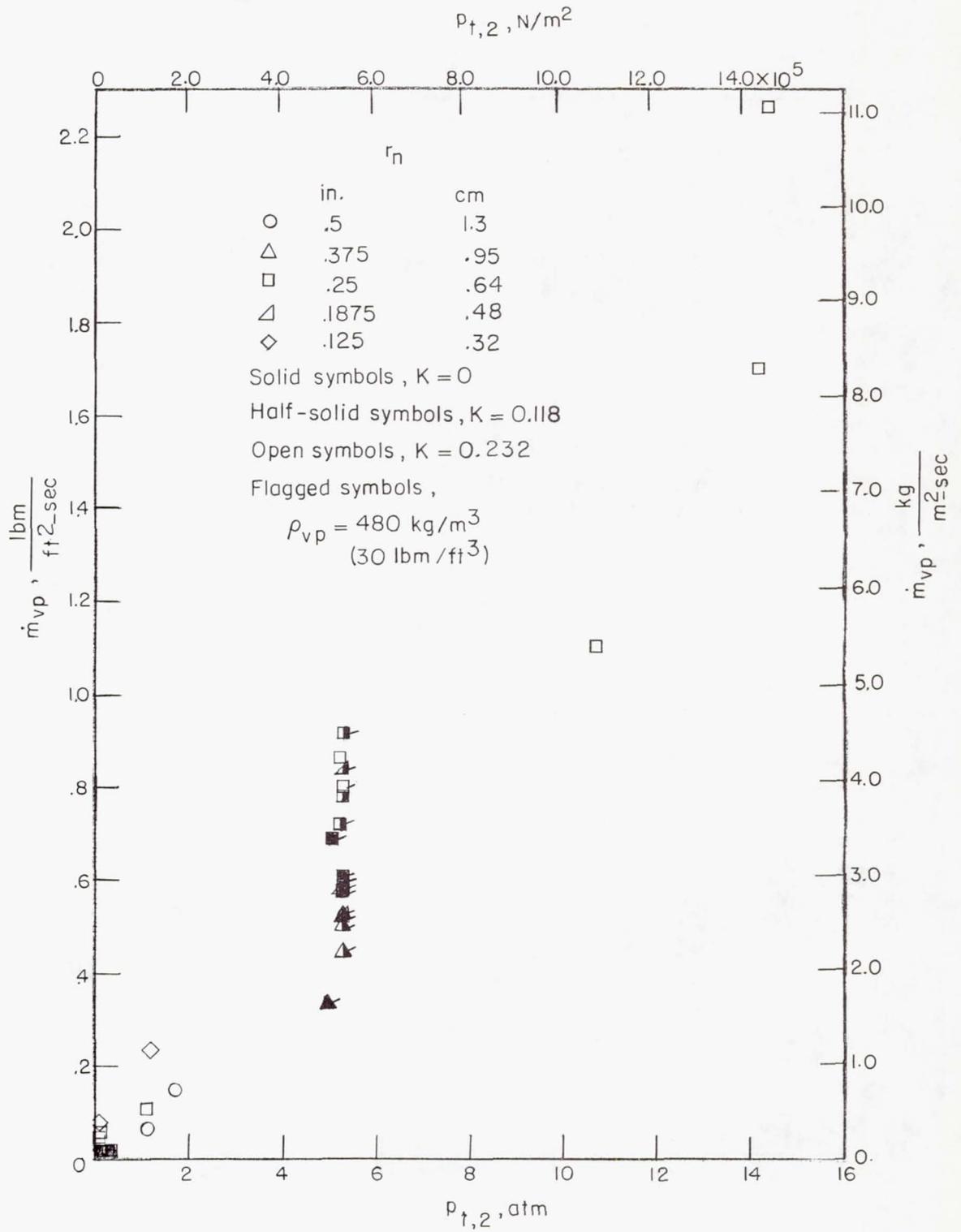
Figure 10.- Mass-loss rate as a function of stagnation pressure for all test runs.
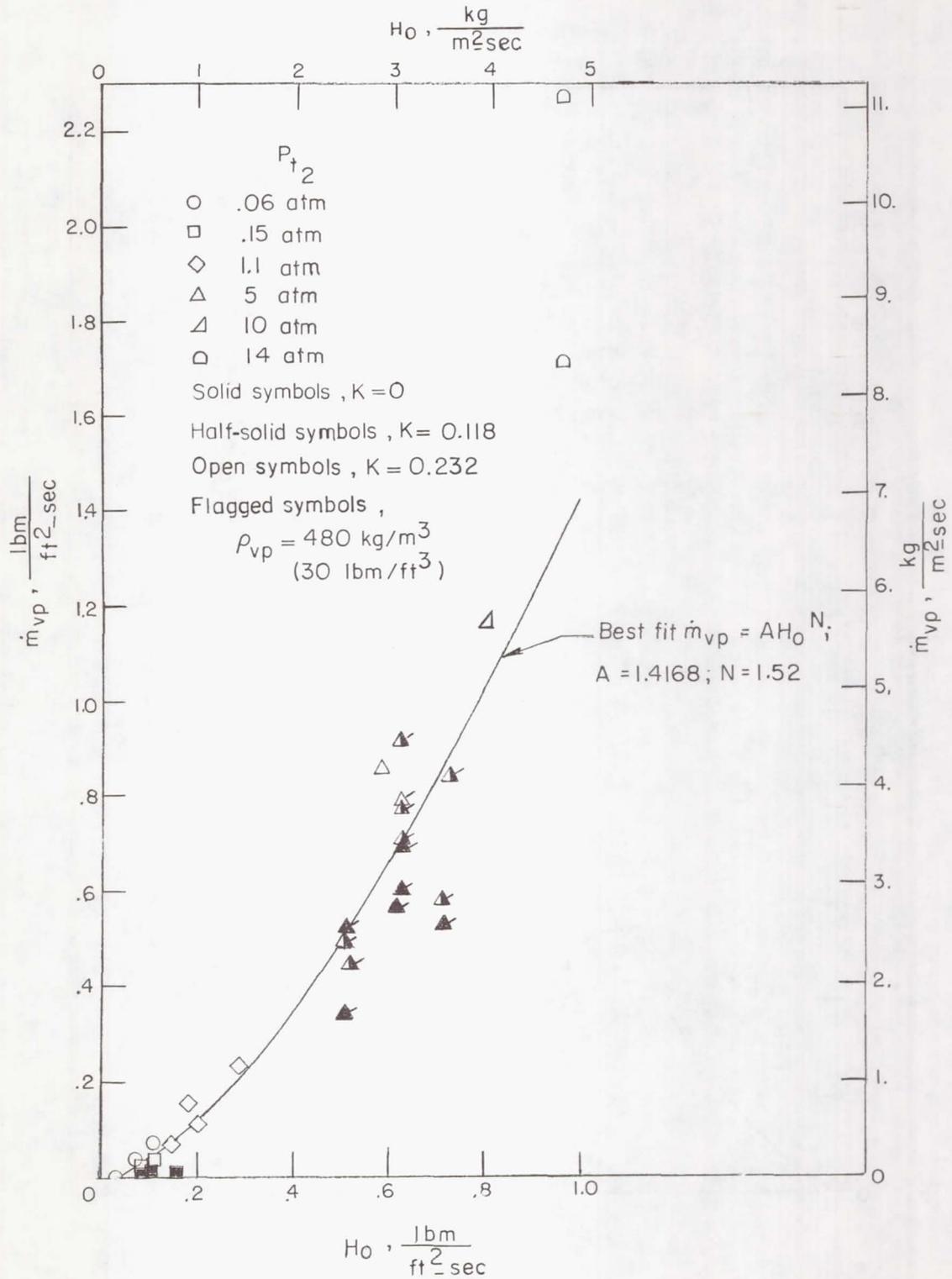
Figure 11.- Mass-loss rate as a function of heat-transfer coefficient for all test runs.
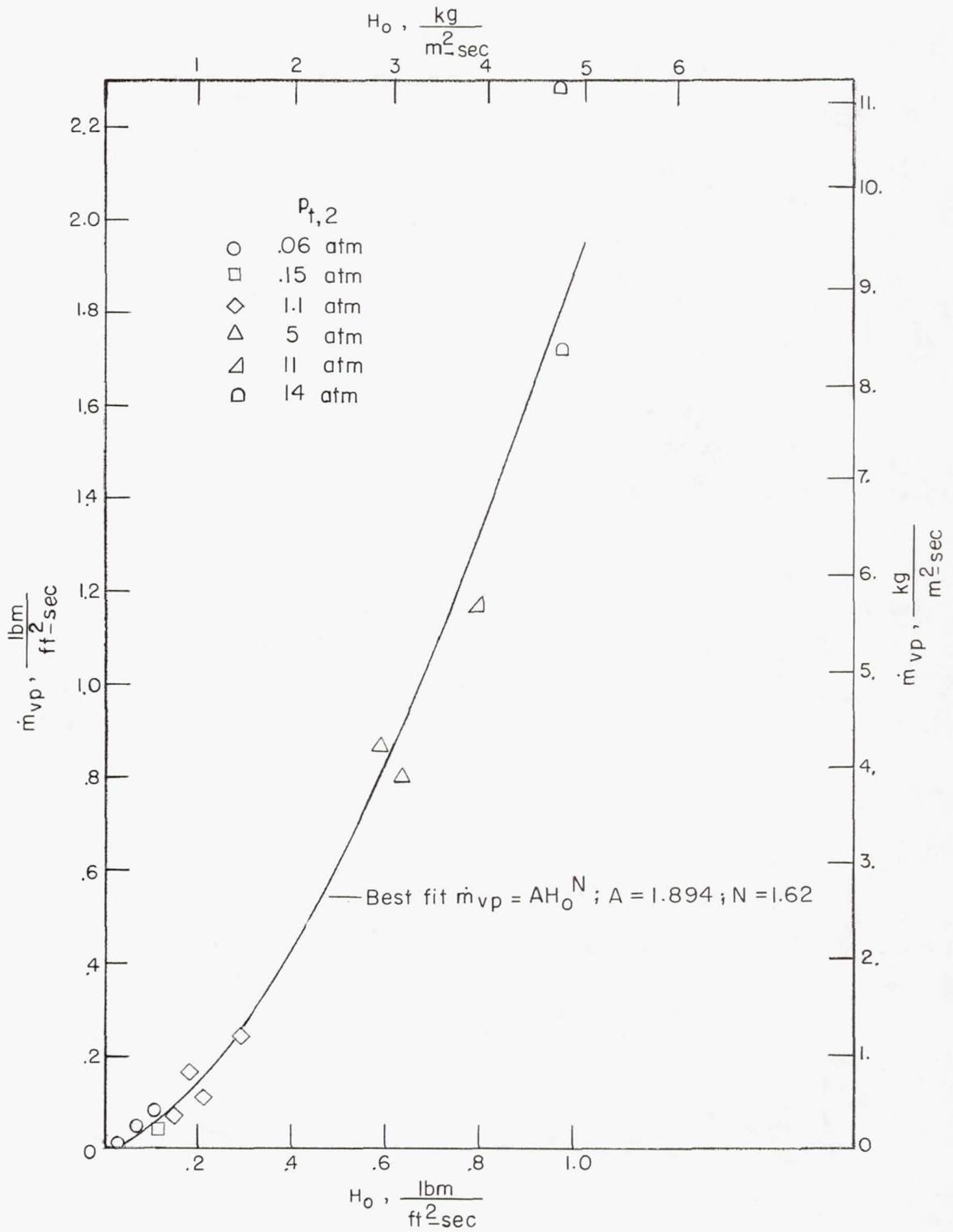
Figure 12.- Mass-loss rate as a function of heat-transfer coefficient for test runs in air.
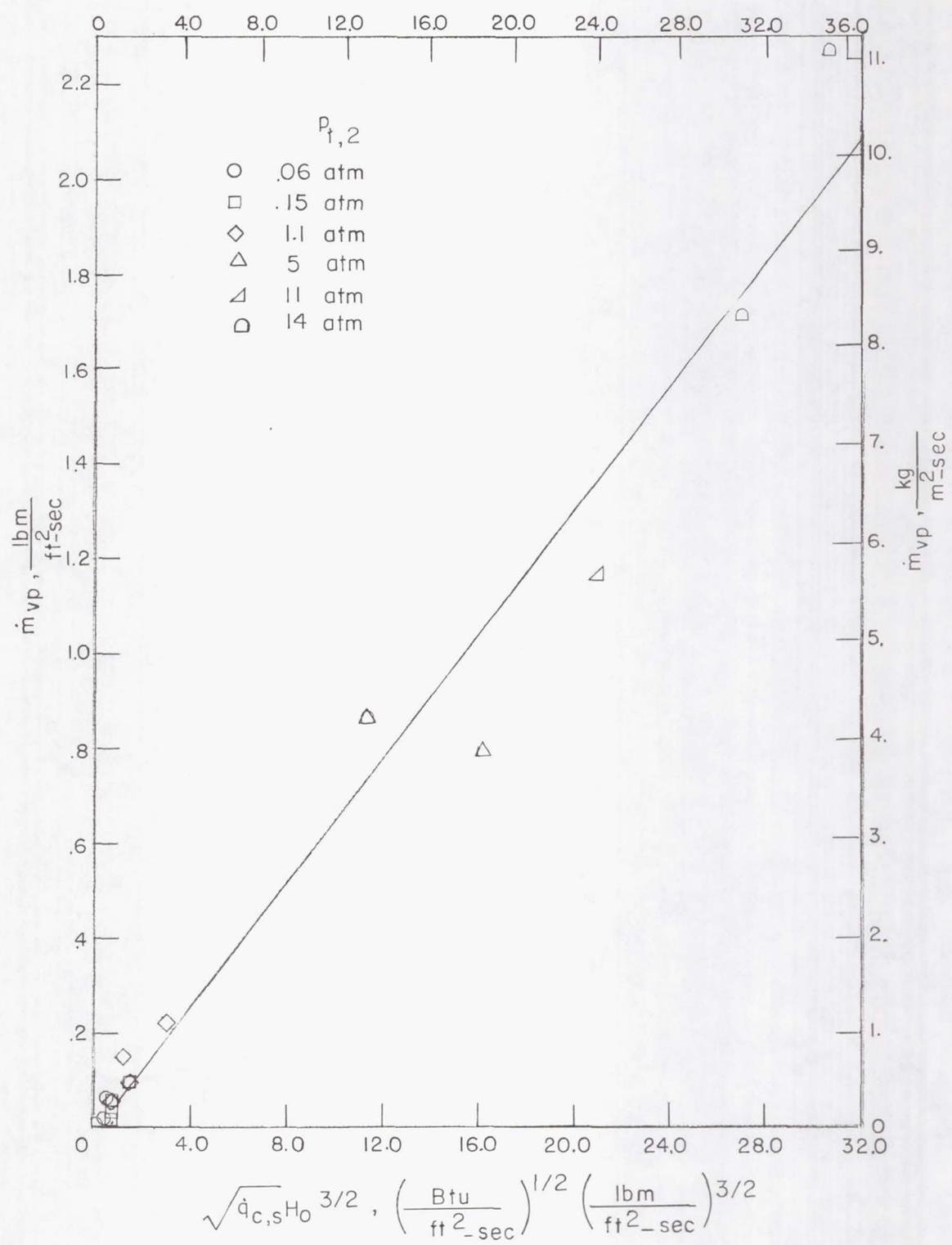
Figure 13.- Mass-loss rate as a function of oxygen-shear product for test runs in air.